American Mineralogist, Volume 88, pages 80–86, 2003

Thermal equation of state of omphacite

YU NISHIHARA,[1,*] EIICHI TAKAHASHI,[1] KYOKO MATSUKAGE,[2] AND TAKUMI KIKEGAWA[3]

[1]Magma Factory, Earth and Planetary Sciences, Tokyo Institute of Technology, Ookayama, Meguro-ku, Tokyo 152–8551, Japan
[2]Department of Environmental Sciences, Ibaraki University, Bunkyo, Mito, Ibaraki 310–8512, Japan
[3]High Energy Accelerator Research Organization, Oho, Tsukuba, Ibaraki 305–0801, Japan

ABSTRACT

In-situ synchrotron X-ray diffraction experiments were conducted using the MAX-III multi-anvil press of KEK on an omphacite ($Di_{63}Jd_{37}$), for which Di = $Ca(Mg,Fe)Si_2O_6$ and Jd = $NaAlSi_2O_6$. Pressure-volume-temperature data were collected at up to 10 GPa and 1000 K. A fit to the high-temperature Birch-Murnaghan equation of state yielded an isothermal bulk modulus K_{T0} = 126(1) GPa, an assumed pressure derivative of the bulk modulus K_T' = 4.0, a temperature derivative of the bulk modulus $(\partial K_T/\partial T)_P$ = –0.015(4) GPa/K, and a volumetric thermal expansivity $\alpha = 2.2(1) \times 10^{-5}$ K^{-1}, when the equation of state of NaCl by Brown (1999) is adopted for the pressure scale. The derived K_{T0} value is consistent with the linear interpolations from K_{T0} values for diopside and jadeite in the literature.

INTRODUCTION

Subducted mid oceanic ridge basalt (MORB), which is rich in components of pyroxene and garnet, may be the source of the most important chemical heterogeneity in the olivine-rich Earth's mantle. It is well understood that the MORB component exists as eclogite at pressure conditions of 3–15 GPa (e.g., Irifune et al. 1986). Omphacitic clinopyroxene, which consists essentially of solid solution of a diopside ($CaMgSi_2O_6$) and jadeite ($NaAlSi_2O_6$), is the major mineral phase in eclogite. Knowledge of the physical properties of omphacite is very important in clarifying the behavior of subducted MORB in the deep mantle.

Some experimental results have been reported for density changes of omphacites at high-temperature or high-pressure (McCormick et al. 1989; Pavese et al. 2000, 2001). McCormick et al. (1989) conducted room-temperature compression experiments to 6 GPa with the diamond-anvil cell using a liquid pressure medium on both vacancy-rich and vacancy-poor natural omphacites, and Pavese et al. (2001) reported similar experiments to 13 GPa on a *P*2/*n*-omphacite. Pavese et al. (2000) recorded thermal expansive properties for the same *P*2/*n*-omphacite that was used in Pavese et al. (2001). Thermal equation of states on some end-member clinopyroxenes have also been investigated (e.g., diopside; Zhao et al. 1998, jadeite; Zhao et al. 1997). However, simultaneous in situ measurements of thermoelastic properties of omphacite at high-pressure and high-temperature are still needed to derive complete equation of state for this mineral.

In this study, pressure-volume-temperature (*P*-*V*-*T*) relations of synthetic omphacite were measured at pressure and temperature conditions up to 10 GPa and 1000 K with synchrotron radiation, and the thermal equation of state was determined. The results are compared to previously reported thermoelastic parameters of omphacites and end-member pyroxenes.

EXPERIMENTAL PROCEDURE

Samples

Based on the results of the previous phase equilibrium experiments on the MORB composition, we synthesized omphacite to have an appropriate chemical composition for an eclogitic clinopyroxene. Chemical compositions of clinopyroxene in MORB at 5 GPa and 1773 K (Aoki 1999), and at 5.6 GPa and 1473 K (Irifune et al. 1986) are shown in Table 1. Although the experimental conditions and starting compositions are similar, compositions of these two clinopyroxene minerals differ significantly in SiO_2 and Al_2O_3. This may be due to the different starting materials (dried natural MORB in Aoki 1999 vs. glass in Irifune et al. 1986). Reagents were mixed to match the former composition. Trace elements were ignored and reagents of SiO_2, Al_2O_3, Fe_2O_3, MgO, $CaCO_3$, and Na_2CO_3 were used. The mixture was ground and heated slowly from 873 to 1173 K and kept at 1173 K for more than 12 hours for decarbonation. The decarbonated sample was then melted for 10 min at 1622 K at the fayalite-magnetite-quartz buffer in a one atmosphere furnace. The quenched glass was confirmed to be homogeneous by microprobe analysis. Omphacite was synthesized from the glass using the SPI-1000 1000 ton multi-anvil press at the Magma Factory, Tokyo Institute of Technology. The glass was enclosed in a Re foil capsule (3.2 mm in diameter, 3.4 mm in length), and experimental conditions were *P* = 5 GPa, *T* = 1773 K, and *t* = 30 min. Experimental techniques and the cell assembly used in the synthesis

* E-mail: yuu@geo.titech.ac.jp

0003-004X/03/0001–80$05.00

experiments are similar to those of Takahashi et al. (1993) and Tsuruta and Takahashi (1998).

Chemical analyses were done with a JEOL-8800 microprobe. Accelerating voltage and beam current of 15 kV and 12 nA, respectively, were used with counting times of 10 s for the peak and 5 s for the backgrounds on either side of the peak. The standards used were: SiO_2, wollastonite; Al_2O_3, corundum; FeO, hematite; MgO, periclase; CaO, wollastonite; and Na_2O, natural albite. The microprobe analyses showed that most of the sample consisted of omphacite, although minor amounts of garnet and coesite were also identified. The weight ratios of omphacite, garnet, and coesite were calculated to be 87%, 10%, and 4%, respectively, on the basis of mass balance equations. The chemical composition of the synthesized omphacite is listed in Table 2. The omphacite has lower Al_2O_3 and FeO contents than the model clinopyroxene (Aoki 1999, Table 1). This omphacite contains a relatively high content of Ca-Eskola end-member (9 mol% $Ca_{0.5}\square_{0.5}AlSi_2O_6$). After the *P-V-T* experiments, the chemical compositions of the omphacite samples were examined, and no changes were detected.

Angular dispersive X-ray powder diffraction with Cr$K\alpha$ radiation was carried out using the synthesized sample at ambient conditions. The results also showed the existence of minor garnet and coesite. The unit-cell parameters of the omphacite were calculated to be a = 9.607(2) Å, b = 8.774(2) Å, c = 5.254(2) Å, β = 106.85(4)°, and V = 423.8(2) Å^3 from the positions of 20 diffraction peaks. It is well known that the order-disorder phase transition occurs in omphacite (e.g., Carpenter 1980). It is quite difficult to distinguish between *C*2/*c*- and *P*2/*n*-omphacite samples from powder X-ray diffraction, because all the reflections due to ordering are very weak (Clark and Papike 1968). *P*2/*n*-omphacite is stable only at low temperature (< ~700 °C, Carpenter 1980). Judged from its chemical composition and our synthesis conditions, the space group of our omphacite is *C*2/*c* rather than *P*2/*n*. These two structures are quite similar and the phase transition would have no significant effect on the *P-V-T* data.

TABLE 1. Chemical composition of clinopyroxene in MORB

Wt%	Aoki*	Irifune†
SiO_2	53.92	51.60
TiO_2	0.50	0.70
Al_2O_3	12.53	15.71
FeO	6.03	5.36
MnO	0.06	–
MgO	9.33	8.73
CaO	13.58	14.37
Na_2O	3.39	3.20
K_2O	0.04	–
P_2O_5	0.08	–
Total	99.46	99.67

* Clinopyroxene in MORB composition at 5 GPa and 1773 K (Aoki 1999).
† Clinopyroxene in MORB composition at 5.6 GPa and 1473 K (Irifune et al. 1986).

TABLE 2. Chemical composition of omphacite

Chemical analysis			Pyroxene end-members	
Cation	Weight percent oxide	Number of cations (O = 6)	Component	Mole percent
Si	55.08(47)	1.954(12)	$NaAlSi_2O_6$	28.4(19)
Al	11.12(46)	0.465(19)	$CaAl_2SiO_6$	4.6(12)
Fe	4.52(40)	0.134(12)	$Ca_{0.5}\square_{0.5}AlSiO_6$	8.9(37)
Mg	10.40(25)	0.550(13)	$Ca_2Si_2O_6$	23.9(13)
Ca	14.94(40)	0.568(15)	$Mg_2Si_2O_6$	27.5(7)
Na	4.13(28)	0.284(19)	$Fe_2Si_2O_6$	6.7(6)
Total	100.18	3.956		100.0

Note: Estimated standard deviations in parentheses are based on 16 analyses.

P-V-T experiments

P-V-T experiments were conducted using the MAX-III multi-anvil apparatus installed on a synchrotron beam line (BL14C2) at the Photon Factory at the National Laboratory for High Energy Accelerator Research Organization, Tsukuba, Japan. Six sintered diamond anvils (4×4 mm^2 truncation size) were used for high-pressure generation. Figure 1 shows a schematic cross-section of the cell assembly. A cubic pressure medium ($7 \times 7 \times 7$ mm^3) made up of a mixture of boron and epoxy resin (weight ratio 4:1) with a tubular graphite heater was used. Powdered omphacite and a mixture of NaCl and BN (weight ratio 6:1) were packed into the BN sample chamber separately. Temperature was measured with a W5%Re-W26%Re thermocouple, and pressure was determined by the thermal equation of state of NaCl (Decker 1971; Brown 1999).

A solid-state detector connected to a multi-channel analyzer was used for data collection. The multi-channel analyzer was calibrated with the characteristic X-rays of Mo, Ag, Dy, Ta, Au, and Bi. The diffracted X-rays from the sample were collected at a fixed 2θ angle of ~6.0° by the energy dispersive method. The 2θ angle was calibrated with the unit-cell volume of NaCl. The incident X-ray beam was collimated to 0.05 mm and 0.2 mm in the vertical and horizontal dimensions, respectively. Three thin slits between the sample and the detector, 0.05 and 0.2 mm in the vertical dimension and 0.5 mm in horizontal, were used to eliminate diffracted X-rays from the pressure medium. The X-ray diffraction data were collected at positions 0.2 mm above and below the thermocouple junction for the sample and the pressure marker, respectively. Typical exposure times for collecting diffraction patterns of the sample and pressure marker were 600 and 300 s, respectively. Temperature variation indicated by the thermocouple was within 5 K. Figure 2 shows an example of the diffraction spectrum of omphacite. The unit-cell parameters were calculated from peak positions by the least-squares technique. Because of overlapping diffraction peaks from both omphacite and other materi-

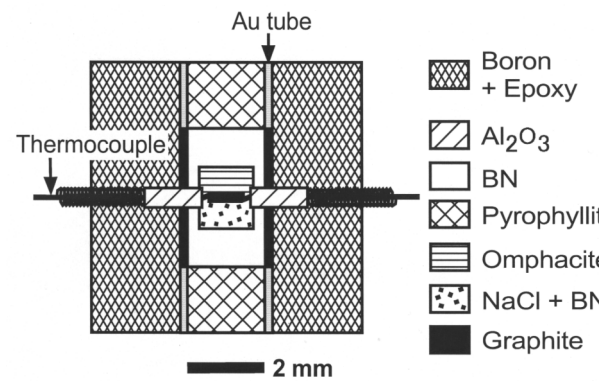

FIGURE 1. Schematic cross section of the cell assembly.

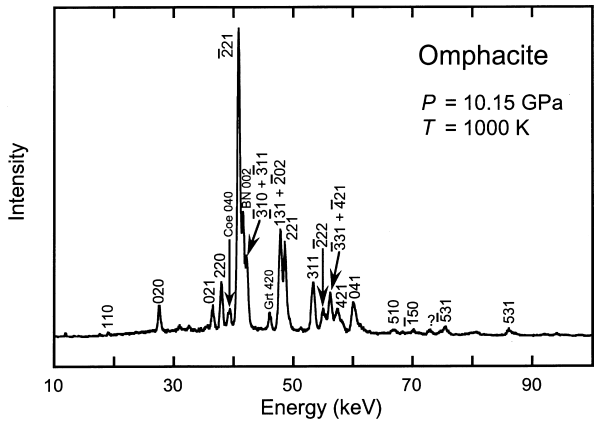

FIGURE 2. Example of diffraction spectra of omphacite at 10.15 GPa (Brown's scale, Brown 1999) and 1000 K. Diffraction peaks for coesite (Coe) and garnet (Grt), which coexist with omphacite, and the sample capsule of boron nitride (BN) are also detected.

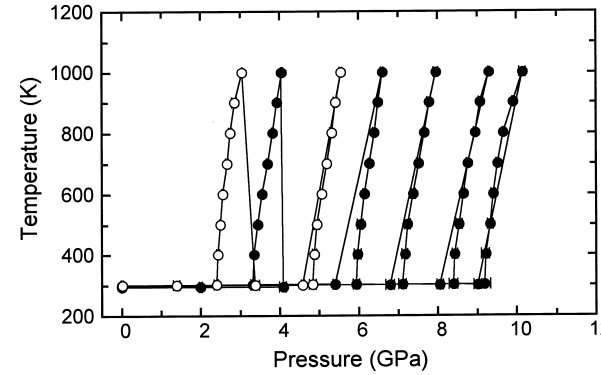

FIGURE 3. Pressure-temperature paths of present experiments. Solid and open circles are experiments no. 1 and no. 2, respectively. The pressures are calculated using the Brown (1999) EOS for NaCl.

als, the number of reflections used was limited to 8–11. The use of 8 to 11 peaks to fix the lattice parameters of a monoclinic symmetry compound results in under-estimation of a, b, c, and β. The pressure was determined from the observed cell volume of NaCl using the pressure scales of Brown (1999) and Decker (1971). The cell volumes of NaCl were calculated from four diffraction lines; 200, 220, 222, and 400. The errors in the calculated pressures were estimated from the difference of calculated pressure from different peaks of NaCl. The estimated errors were 0.04 GPa on average, and 0.15 GPa at the maximum.

Two *P-V-T* experiments (no. 1 and no. 2) were conducted. The sample was compressed to the desired pressure at room temperature and heated to the maximum temperature (1000 K) to release non-hydrostatic stress. X-ray diffraction data for both the sample and the pressure marker were collected at fixed temperatures with 100 K intervals under constant ram load. After the data collection at room temperature, the sample was further compressed, and the heating and data collection cycle was repeated again. The procedure was repeated for up to 7 temperature excursions in two experiments. Figure 3 shows the *P-T* paths in the two experiments. In Figure 3, pressure values calculated by the Brown (1999) equation of state (EOS) are indicated. Brown's EOS yields a revised pressure scale for NaCl proposed as an update to the 30-year-old work of Decker (1971). As mentioned by Brown (1999), the pressure differences between these two scales are larger at higher pressure and lower temperature. Although the pressure differences are not so great (<0.3 GPa), they affect significantly the derived EOS of omphacite. In this study, the pressure values based on Brown's pressure scale were used after comparison with those based on Decker's scale.

RESULTS AND DISCUSSION

Thermal equation of state

The unit-cell parameters of omphacite at various *P-T* conditions are given in Table 3. Only the data collected during cooling (and data at ambient conditions), which are considered to be closer to hydrostatic conditions, are listed in Table 3 and used in subsequent calculations. Figure 4 shows the volume data measured at 300, 500, 700, 900, and 1000 K.

The high-temperature Birch-Murnaghan (HTBM) equation of state is often used to fit the *P-V-T* data (e.g., Funamori et al. 1996; Wang et al. 1998). The equation of state is given by the following expression:

$$P = 3/2K_T\left[(V_{0T}/V)^{7/3} - (V_{0T}/V)^{5/3}\right]\left\{1 + 3/4\left(K_T' - 4\right)\left[(V_{0T}/V)^{2/3} - 1\right]\right\} \quad (1)$$

where K_T, V_{0T}, V, and K_T' are the isothermal bulk modulus, zero-pressure volume, high-pressure volume, and pressure derivative of K_T, respectively. The temperature effects for K_T and V_{0T} are expressed as follows:

$$K_T = K_{T0} + (\partial K_T/\partial T)_P(T - 300) \quad (2)$$

$$V_{0T} = V_0 \exp\left[\int_{300}^{T} \alpha \mathrm{d}T\right] \quad (3)$$

where $(\partial K_T/\partial T)_P$ and α are the temperature derivative of the bulk modulus and the volumetric thermal expansion at atmospheric pressure, respectively. The α, K_T', and $(\partial K_T/\partial T)_P$ values are assumed to be constant. In the case of angle dispersive X-ray diffraction, the observed diffraction lines are relatively sharp and the overlap of diffraction lines is not so great, compared with the case of energy dispersive X-ray diffraction. Thus, the V_{0T} value determined by the angle dispersive method is expected to be more accurate. In the following calculations, V_{0T} was fixed to be the value determined by angle dispersive X-ray diffraction (V_{0T} = 423.8 Å^3).

The experimental *P-V-T* data (Table 3) were fitted to HTBM equation of state, and results are listed in Table 4. The fits without constraint on K_T' yielded relatively high values of K_T' ($K_T' \approx$ 7). However, the limited pressure range and limited precision of volume data in our experiments prevented us from resolving the K_T' value with confidence. We also calculated the equation of state by fixing K_T' at 4 and 5. $K_T' = 4$ is the most common value for silicate minerals and corresponds to a second-order

TABLE 3. Unit-cell parameters of omphacite at various *P-T* conditions

P_B* (GPa)	P_D† (GPa)	*T* (K)	*a* (Å)	*b* (Å)	*c* (Å)	β (°)	*V* (Å³)
				Experiment no. 1			
0.00	0.00	294	9.596(7)	8.765(2)	5.277(8)	106.89(8)	424.7(7)
4.05	4.05	1000	9.553(2)	8.721(4)	5.214(4)	106.62(2)	416.2(4)
3.94	3.94	900	9.546(4)	8.718(7)	5.211(7)	106.63(4)	415.5(7)
3.82	3.81	800	9.546(3)	8.711(5)	5.214(5)	106.64(3)	415.4(5)
3.70	3.69	700	9.536(2)	8.709(5)	5.213(4)	106.60(2)	414.9(4)
3.55	3.52	600	9.533(4)	8.703(7)	5.209(7)	106.59(4)	414.2(7)
3.45	3.41	500	9.530(3)	8.699(6)	5.211(5)	106.58(3)	414.1(5)
3.36	3.29	400	9.527(3)	8.690(6)	5.210(6)	106.55(3)	413.5(6)
3.32	3.23	303	9.526(9)	8.687(18)	5.215(17)	106.67(9)	413.4(17)
6.61	6.58	1000	9.485(9)	8.681(5)	5.174(18)	106.52(14)	408.5(14)
6.49	6.45	900	9.475(6)	8.675(3)	5.172(11)	106.37(9)	407.9(9)
6.40	6.35	800	9.483(8)	8.667(5)	5.171(15)	106.45(12)	407.6(12)
6.27	6.21	700	9.469(6)	8.667(4)	5.168(12)	106.36(10)	407.0(10)
6.15	6.07	600	9.466(6)	8.658(3)	5.171(11)	106.36(9)	406.7(9)
6.05	5.94	500	9.465(3)	8.650(2)	5.172(6)	106.26(4)	406.5(5)
5.98	5.85	400	9.470(4)	8.649(2)	5.168(8)	106.31(6)	406.2(7)
5.94	5.77	303	9.463(5)	8.647(3)	5.166(9)	106.29(7)	405.7(7)
7.96	7.91	1000	9.456(7)	8.650(4)	5.155(13)	106.38(10)	404.6(11)
7.78	7.72	900	9.450(4)	8.641(2)	5.161(7)	106.28(6)	404.5(6)
7.66	7.58	800	9.445(5)	8.639(3)	5.157(9)	106.26(7)	404.0(8)
7.52	7.42	700	9.446(4)	8.633(2)	5.159(7)	106.23(5)	403.9(6)
7.38	7.27	600	9.449(4)	8.626(3)	5.158(8)	106.29(7)	403.5(7)
7.23	7.09	500	9.441(4)	8.625(2)	5.154(7)	106.18(5)	403.1(6)
7.17	7.00	400	9.437(3)	8.616(2)	5.157(6)	106.14(4)	402.8(5)
7.11	6.89	303	9.441(4)	8.611(2)	5.155(7)	106.18(5)	402.5(6)
9.31	9.23	1000	9.441(6)	8.603(3)	5.155(11)	106.38(9)	401.7(9)
9.08	8.99	900	9.432(5)	8.604(3)	5.150(9)	106.23(8)	401.3(7)
8.95	8.84	800	9.429(4)	8.600(2)	5.150(8)	106.14(6)	401.2(6)
8.77	8.64	700	9.420(5)	8.594(3)	5.154(9)	106.05(8)	400.9(8)
8.66	8.51	600	9.418(4)	8.584(2)	5.165(8)	106.18(7)	401.1(7)
8.55	8.37	500	9.421(3)	8.592(2)	5.148(6)	106.16(5)	400.2(5)
8.44	8.23	400	9.418(4)	8.583(2)	5.155(7)	106.20(6)	400.2(6)
8.40	8.15	302	9.421(4)	8.582(2)	5.149(8)	106.20(7)	399.8(6)
10.15	10.06	1000	9.425(3)	8.590(2)	5.142(5)	106.29(4)	399.6(4)
9.92	9.81	900	9.416(3)	8.590(2)	5.144(6)	106.19(4)	399.6(4)
9.67	9.54	800	9.426(4)	8.583(2)	5.152(8)	106.25(6)	400.2(6)
9.53	9.38	700	9.423(5)	8.578(3)	5.150(10)	106.27(7)	399.6(8)
9.41	9.23	600	9.419(5)	8.574(3)	5.149(10)	106.25(8)	399.2(8)
9.34	9.13	500	9.424(6)	8.569(3)	5.148(11)	106.27(9)	399.0(9)
9.22	8.98	400	9.417(6)	8.568(3)	5.143(11)	106.24(9)	398.4(9)
9.20	8.92	302	9.419(5)	8.568(3)	5.131(11)	106.23(8)	397.6(9)
0.00	0.00	299	9.603(3)	8.770(1)	5.259(4)	106.87(4)	423.8(4)
				Experiment no. 2			
0.00	0.00	300	9.603(3)	8.767(2)	5.271(6)	106.81(5)	424.8(5)
3.06	3.07	1000	9.569(2)	8.763(1)	5.239(3)	106.62(2)	421.0(3)
2.86	2.87	900	9.565(2)	8.758(1)	5.233(4)	106.57(3)	420.2(3)
2.76	2.77	800	9.560(2)	8.750(1)	5.236(3)	106.59(2)	419.7(3)
2.67	2.67	700	9.562(1)	8.745(0)	5.233(2)	106.62(1)	419.3(1)
2.56	2.55	600	9.557(1)	8.742(1)	5.230(2)	106.60(1)	418.7(2)
2.50	2.47	500	9.552(2)	8.734(1)	5.230(3)	106.58(2)	418.2(2)
2.44	2.40	400	9.541(1)	8.731(1)	5.229(2)	106.56(2)	417.6(2)
2.40	2.34	303	9.541(1)	8.723(1)	5.230(2)	106.57(2)	417.2(2)
5.56	5.55	1000	9.506(4)	8.704(2)	5.192(8)	106.38(6)	412.2(7)
5.42	5.40	900	9.505(4)	8.698(2)	5.191(8)	106.38(6)	411.7(7)
5.32	5.30	800	9.501(5)	8.692(3)	5.190(10)	106.38(7)	411.2(8)
5.20	5.16	700	9.502(5)	8.690(3)	5.186(9)	106.39(7)	410.8(7)
5.07	5.01	600	9.499(4)	8.685(2)	5.185(8)	106.37(6)	410.4(6)
4.95	4.88	500	9.500(5)	8.680(3)	5.186(10)	106.43(8)	410.1(8)
4.89	4.79	400	9.498(7)	8.675(4)	5.188(13)	106.48(10)	409.9(11)
4.84	4.70	303	9.487(5)	8.673(3)	5.188(10)	106.40(7)	409.5(8)
0.02	0.02	300	9.603(3)	8.767(2)	5.271(6)	106.81(5)	424.8(5)

* Pressure scale by Brown (1999).
† Pressure scale by Decker (1971).

TABLE 4. Thermoelastic parameters of omphacite

	Parameters					
Pressure Scale	Brown	Brown	Brown	Decker	Decker	Decker
K_{T0} (GPa)	117(4)	126(1)	123(1)	114(4)	123(1)	119(1)
K_T'	6.9(12)	[4]	[5]	6.7(11)	[4]	[5]
$(\partial K_T/\partial T)_P$ (GPa/K)	–0.026(5)	–0.015(4)	–0.019(3)	–0.024(5)	–0.013(4)	–0.018(3)
α (10^{-5} K^{-1})	2.7(3)	2.2(1)	2.4(1)	2.8(3)	2.3(1)	2.5(1)

Notes: V_{0T} is fixed to be 423.8 Å³ in the calculation. Square brackets indicate fixed parameters in the fit.

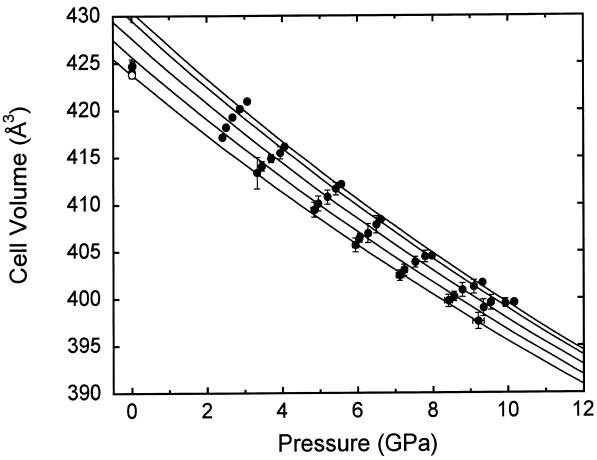

FIGURE 4. *P-V-T* data of omphacite with calculated isothermal compression curves. Open circle is the result of angle dispersive X-ray diffraction at ambient condition. Pressures are based on Brown's scale (Brown 1999). Data collected at 300 K, 500 K, 700 K, 900 K, and 1000 K are shown. The isotherms (from lower cell volumes, 300, 500, 700, 900, 1000 K) are calculated from thermoelastic parameters derived at $K'_T = 4.0$ (Table 4).

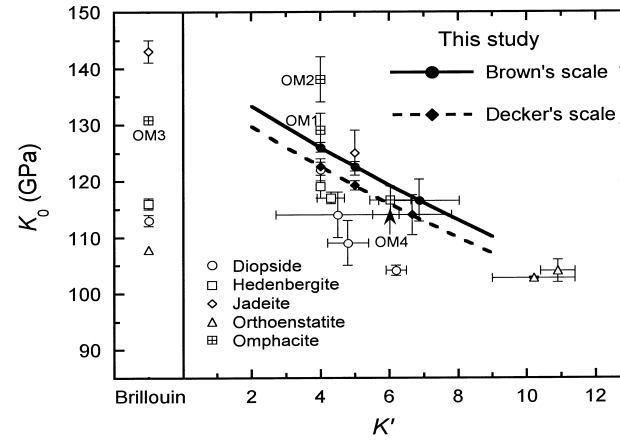

FIGURE 5. Dependence of K_0 on K' values for omphacite and comparison to other pyroxene species. Bold (solid and broken) lines represent the dependencies of K_{T0} on fixed K'_T. Solid symbols are fitted K_{T0} values without constraint on K'_T, and at $K'_T = 4.0$ and 5.0 (Table 4). Solid lines and solid circles are based on Brown's scale (Brown 1999). Broken lines and solid diamonds are based on Decker's scale (Decker 1971). Open symbols are diopside (circles, Levien et al. 1979; Levien and Prewitt 1981; McCormick et al. 1989; Zhang et al. 1997; Zhao et al. 1998), hedenbergite (squares, Kandelin and Weidner 1988a; Zhang and Hafner 1992; Zhang et al. 1997), jadeite (diamonds, Kandelin and Weidner 1988b; Zhao et al. 1997), orthoenstatite (triangles, Weidner et al. 1978; Zhao et al. 1995; Flesch et al. 1998) and omphacite [squares with cross, McCormick et al. 1989 (OM1, OM2); Bhagat et al. 1992 (OM3); Pavese et al. 2001 (OM4)]. OM2 and OM3 have identical compositions. Data plotted in the left box are the results of Brillouin scattering measurements (K_{S0}) at ambient conditions and their K' are not determined. Previous high-*P* XRD results are comparable with present results based on Decker's scale (Decker 1971).

Birch Murnaghan equation of state. Similar to this study, Zhao et al. (1997, 1998) conducted *P-V-T* experiments on jadeite and diopside, and their results showed $K'_T \approx 5$. For comparison with these previous studies, the K'_T was also fixed at 5. The same calculations were carried out based on the two pressure scales for NaCl (Brown 1999; Decker 1971).

The calculated thermal expansivity α does not change significantly with the value chosen for K'_T. However, the calculated bulk modulus and its temperature derivative depend strongly on the assumed K'_T value. The tradeoffs between K_{T0} and K'_T are indicated in Figure 5. It is well recognized that the calculated K_{T0} value decreases with increasing K'_T. The $(\partial K_T/\partial T)_P$ value also shows a significant correlation with K'_T, and we could not strictly constrain it. Because Brown's scale results in slightly higher pressures than Decker's, the bulk moduli based on Brown's scale are larger than those based on Decker's scale at the same K'_T. The thermal expansivity α does not change significantly with the choice of pressure scale. In Figure 4, the isothermal compression curves calculated from the fitted thermoelastic parameters (Brown's pressure scale, $K'_T = 4$) are illustrated. The differences between the experimental results and calculated compression curves are generally within experimental uncertainties (error bars in Fig. 4).

Figure 6 shows variations of the isothermal bulk modulus K_T for omphacite with temperature at $K'_T = 4.0$. The symbols show the calculated isothermal bulk moduli obtained by fitting the data at each temperature to the Birch-Murnaghan equation of state. The lines are the results of fits to the HTBM equation of state for all of the data. Decreasing K_T with increasing temperature is represented by linear expression. In Figure 6, both data based on Brown's (1999) scale and Decker's (1971) scale are plotted. Because the differences of pressure values between these two pressure scales are smaller at higher temperatures, the difference of bulk modulus decreases with increasing tem-

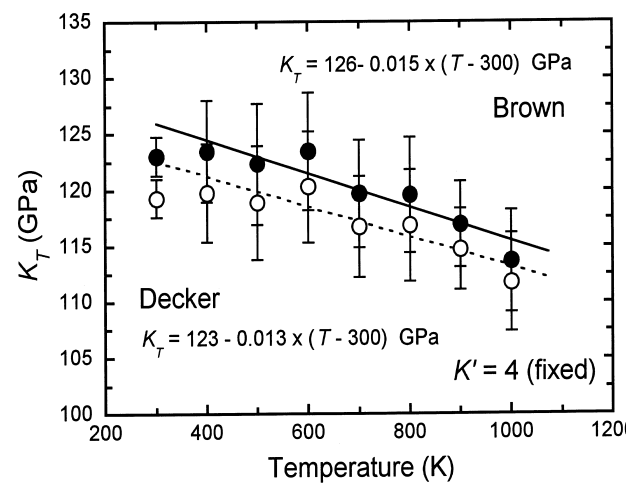

FIGURE 6. Variations of the isothermal bulk modulus for omphacite against temperature. Circles are isothermal bulk moduli calculated by fitting the data at each temperature. Lines are the results of fits to the HTBM equation of state (Table 4). Solid circles and the solid line are based on Brown's scale (Brown 1999); open circles and the broken line are based on Decker's scale (Decker 1971). K'_T is fixed to be 4.0 in the calculations.

perature. As indicated in Table 4, this feature is expressed as larger absolute values of $(\partial K_T/\partial T)_P$ when Brown's scale is used.

COMPARISON WITH OTHER PYROXENES

Elastic properties of pyroxene minerals have been investigated by various experimental methods. Most of the studies are based on X-ray diffraction (XRD) at high-pressure and Brillouin scattering at ambient conditions. The compression curve from which the isothermal bulk modulus and its pressure derivative can be determined is obtained by XRD at high P. The calculated bulk moduli and their pressure derivatives are generally highly dependent on each other because of the limited experimental pressure range and the precision of volume data as described for our results (Table 4 and Fig. 5). The elastic constants are derived from the single-crystal Brillouin scattering, and from these the adiabatic bulk and shear moduli at ambient conditions can be determined. The relation between isothermal and adiabatic bulk moduli (K_T and K_S, respectively) is expressed as follows: $K_T = K_S/(1 + \alpha\gamma_G T)$ where α and γ_G are thermal expansivity and the Grüneisen parameter. Because the term $\alpha\gamma_G T$ is estimated to be ~0.01 for pyroxene at 300 K and the difference between K_T and K_S at ambient conditions is similar in size to experimental uncertainties for bulk moduli, K_T and K_S, and are not distinguished in the following discussion.

As noted above, the choice of pressure scale significantly affects the derived bulk modulus in the high-P XRD studies. Most of previous studies are based on Decker's (1971) NaCl pressure scale or on the ruby scale (e.g., Piermarini et al. 1975; Mao et al. 1986). The ruby scale is related to the Decker scale since Piermarini et al. (1975) calibrated ruby fluorescence wavelength shifts against NaCl volumes determined by X-ray diffraction. The ultra high-pressure ruby calibrations (e.g., Mao et al. 1986) use a functional representation that forces a match to Piermarini et al.'s pressure derivative at low pressures. Thus, previous results for other pyroxenes are comparable with the present results based on Decker's scale.

The comparison of the bulk modulus at the ambient condition K_0 and its pressure derivative K' for some end-member pyroxenes (diopside; $CaMgSi_2O_6$, hedenbergite; $CaFeSi_2O_6$, jadeite; $NaAlSi_2O_6$ and orthoenstatite; $Mg_2Si_2O_6$) and omphacites is shown in Figure 5. Data plotted in the left-hand box are the results from Brillouin scattering measurements and their K' were not determined. All the data in the right-hand box are the results from high-pressure XRD except for a datum for orthoenstatite (obtained by ultrasonic interferometry, Flesch et al. 1998). The stiffer sample would be plotted toward the upper right in the diagram. Othoenstatite, which has a different crystal structure, is characterized by relatively low K_0 and high K' values compared to monoclinic pyroxenes. Diopside and hedenbergite have similar compressibilities. The variation in the results shown by high-pressure XRD of diopside (Levien and Prewitt 1981; McCormick et al. 1989; Zhang et al. 1997; Zhao et al. 1998) may show a tradeoff between K_0 and K'. Only two K_0 values for jadeite are reported and they differ significantly [143(2) GPa, Brillouin scattering by Kandelin and Weidner 1988b, 125(4) GPa at $K' = 5.0$, high-P XRD by Zhao et al. 1997]. The reason for the disagreement is not clear. However, it can be concluded that jadeite is the most incompressible pyroxene end-member.

If we use $Ca(Mg,Fe)Si_2O_6$ and $(Mg,Fe)_2Si_2O_6$ as end-members, instead of $Ca_2Si_2O_6$, $Mg_2Si_2O_6$, and $Fe_2Si_2O_6$, the contents of both components in our omphacite are 47.8(27) and 10.3(16) mol%, respectively. In this case, the dominant components are $Ca(Mg,Fe)Si_2O_6$ and $NaAlSi_2O_6$. The contents of Di + Jd are 76 mol% in the clinopyroxene solid solution, and Di and Jd represent $Ca(Mg,Fe)Si_2O_6$ and $NaAlSi_2O_6$, respectively. If we ignore the other components and normalize to 100%, the composition of our omphacite can be expressed as $Di_{63}Jd_{37}$. Assuming a linear relationship between K_0 and composition, and using the results from Brillouin scattering of diopside [K_{S0} = 113(1) GPa, Levien et al. 1979] and jadeite [K_{S0} = 143(2) GPa, Kandelin and Weidner 1988b] to interpolate the bulk modulus for $Di_{63}Jd_{37}$, one calculates $K_0 \approx 124$ GPa. The same interpolation using the results from high-pressure and high-temperature XRD [diopside, K_{T0} = 109(4) GPa, Zhao et al. 1998; jadeite, K_{T0} = 125(4) GPa, Zhao et al. 1997] yields $K_0 \approx 115$ GPa. These are generally consistent with the results of the present experiments (see Table 4).

The omphacites in Figure 5 are expressed as $Di_{24}Jd_{76}$ (OM1; vacancy-rich omphacite by McCormick et al. 1989, 75 mol% Di + Jd content), $Di_{34}Jd_{66}$ (OM2 and 3; McCormick et al. 1989 and Bhagat et al. 1992, 88 mol%) and $Di_{51}Jd_{49}$ (OM4; $P2/n$-omphacite from Pavese et al. 2001, 91 mol%). OM2 and OM3 have identical compositions.

McCormick et al. (1989) performed single crystal XRD experiments at high pressures on samples OM1 and OM2 using a multiple crystal mount in diamond anvil cell. OM2 shows higher K_0 than OM1 in spite of its lower jadeite content. However, this is attributable to the higher Ca-Eskola ($Ca_{0.5}\square_{0.5}AlSi_2O_6$, vacancy-rich end-member) content (13 mol%) in OM1 (McCormick et al. 1989). It should be pointed out that their results [diopside, K_0 = 122(2) GPa; OM2, 139(4) GPa at K' = 4.0] show higher bulk moduli than those obtained by Brillouin scattering from the same materials (diopside, Levien et al. 1979; OM3, Bhagat et al. 1992). The reason for the discrepancy in bulk modulus is unclear. As described in Bhagat at al. (1992), K_0 of OM3 can be explained by interpolation from the results of the Brillouin scattering on diopside and jadeite. Similarly, K_0 of OM4 and the interpolation from the results of the high-pressure and high-temperature XRD show fairly good consistency (Pavese et al. 2001).

Pavese et al. (2000) measured the thermal expansivity of an omphacite, which is the same specimen used by Pavese et al. (2001) for high-P XRD (OM4), from 298 to 1273 K at ambient pressure. The results are $\alpha = 2.76(4)$ and $2.51(3) \times 10^{-5}$/K upon heating and on cooling, respectively, and are consistent with the results of the present experiments (Table 4).

Our data provide a direct assessment of thermoelastic behavior of omphacite at simultaneous high-pressure and high-temperature. Although our omphacite contains some minor end-member components (including vacancy-bearing $Ca_{0.5}\square_{0.5}AlSi_2O_6$) other than diopside and jadeite, the results are generally consistent with a linear interpolation from the thermoelastic parameters of diopside and jadeite given in the literature.

ACKNOWLEDGMENTS

We thank N. Nishiyama, T. Yagi, K. Kusaba, and I. Aoki for their advice on experimental techniques, and T. Iguchi, K. Nakayama, M. Shirasaka, Y. Tange, K. Hirose, and K. Kawamura for their helpful support for the in situ X-ray diffraction experiments. We also thank T. Tsuchiya for useful discussions and T.L. Wright for reading the manuscript. Critical reviews by Y. Wang and A. Pavese helped improve the manuscript. The in-situ X-ray diffraction experiments were performed at the National Laboratory for High Energy Accelerator Research Organization (no. 00G030). Y.N. is grateful for the Research Fellowships of the Japan Society of the Promotion of Science for Young Scientists.

REFERENCES CITED

Aoki, I. (1999) Density of subducted oceanic crust (MORB) in the deep mantle. M.S. Thesis, Tokyo Institute of Technology.

Bhagat, S.S., Bass, J.D., and Smyth, J.R. (1992) Single-crystal elastic properties of omphacite-C2/c by Brillouin spectroscopy. Journal of Geophysical Research, 97, 6843–6848.

Brown, J.M. (1999) The NaCl pressure standard. Journal of Applied Physics, 86, 5801–5808.

Carpenter, M.A. (1980) Mechanisms of exsolution in sodic pyroxenes. Contributions to Mineralogy and Petrology, 71, 289–300.

Clark, J.R. and Papike J.J. (1968) Crystal-chemical characterization of omphacites. American Mineralogist, 53, 840–868.

Decker, D.L. (1971) High-pressure equation of state for NaCl, KCl, and CsCl. Journal of Applied Physics, 42, 3239–3244.

Flesch, L.M., Li, B., and Liebermann, R.C. (1998) Sound velocities of polycrystalline $MgSiO_3$-orthopyroxene to 10 GPa at room temperature. American Mineralogist, 83, 444–450.

Funamori, N., Yagi, T., Utsumi, W., Kondo, T., Uchida, T., and Funamori, M. (1996) Thermoelastic properties of $MgSiO_3$ perovskite determined by in situ X ray observations up to 30 GPa and 2000 K. Journal of Geophysical Research, 101, 8257–8269.

Irifune, T., Sekine, T., Ringwood, A.E., and Hibberson, W.O. (1986) The eclogite-garnetite transformation at high pressure and some geophysical implications. Earth and Planetary Science Letters, 77, 245–256.

Kandelin, J. and Weidner, D.J. (1988a) Elastic properties of hedenbergite. Journal of Geophysical Research, 93, 1063–1072.

——— (1988b) The single-crystal elastic properties of jadeite. Physics of the Earth and Planetary Interiors, 50, 251–260.

Levien, L. and Prewitt, C.T. (1981) High-pressure structural study of diopside. American Mineralogist, 66, 315–323.

Levien, L., Weidner, D.J., and Prewitt, C.T. (1979) Elasticity of diopside. Physics and Chemistry of Minerals, 4, 105–113.

Mao, H.K., Xu, J., and Bell, P.M. (1986) Calibration of the ruby pressure gauge to 800 kbar under quasi-hydrostatic conditions. Journal of Geophysical Research, 91, 4673–4676.

McCormick, T.C., Hazen, R.M., and Angel, R.J. (1989) Compressibility of omphacite to 60 kbar: Role of vacancies. American Mineralogist, 74, 1287–1292.

Pavese, A., Bocchio, R., and Ivaldi, G. (2000) In situ high temperature single crystal X-ray diffraction study of a natural omphacite. Mineralogical Magazine, 64, 983–993.

Pavese, A., Diella, V., Levy, D., and Hanfland, M. (2001) Synchrotron X-ray powder diffraction study of natural P2/n-omphacites at high-pressure conditions. Physics and Chemistry of Minerals, 28, 9–16.

Piermarini, G.J., Block, S., Barnett, J.D., and Forman, R.A. (1975) Calibration of the pressure dependence of the R_1 ruby fluorescence line to 195 kbar. Journal of Applied Physics, 46, 2774–2780.

Takahashi, E., Shimazaki, T., Tsuzaki, Y., and Yoshida, H. (1993) Melting study of a peridotite KLB-1 to 6.5 GPa, and the origin of basaltic magmas. Philosophical Transactions of the Royal Society of London A, 342, 105–120.

Tsuruta, K. and Takahashi, E. (1998) Melting study of an alkali basalt JB-1 up to 12.5 GPa: behavior of potassium in the deep mantle. Physics of the Earth and Planetary Interiors, 107, 119–130.

Wang, Y., Weidner, D.J., Zhang, J., Gwanmesia, G.D., and Liebermann, R.C. (1998) Thermal equation of state of garnets along the pyrope-majorite join. Physics of the Earth and Planetary Interiors, 105, 59–71.

Weidner, D.J., Wang, H., and Ito, J. (1978) Elasticity of orthoenstatite. Physics of the Earth and Planetary Interiors, 17, P7–P13.

Zhang, L. and Hafner, S.S. (1992) High-pressure ^{57}Fe g resonance and compressibility of $Ca(Fe,Mg)Si_2O_6$ clinopyroxenes. American Mineralogist, 77, 462–473.

Zhang, L., Ahsbahs, H., Hafner, S.S., and Kutoglu, A. (1997) Single-crystal compression and crystal structure of clinopyroxene up to 10 GPa. American Mineralogist, 82, 245–258.

Zhao, Y., Schiferl, D., and Shankland, T.J. (1995) A high P-T single-crystal X-ray diffraction study of thermoelasticity of $MgSiO_3$ orthoenstatite. Physics and Chemistry of Minerals, 22, 393–398.

Zhao, Y., Von Dreele, R.B., Shankland, T.J., Weidner, D.J., Zhang, J., Wang, Y., and Gasparik, T. (1997) Thermoelastic equation of state of jadeite $NaAlSi_2O_6$: An energy-dispersive Rietveld refinement study of low symmetry and multiple phases diffraction. Geophysical Research Letters, 24, 5–8.

Zhao, Y., Von Dreele, R.B., Zhang, J.Z., and Weidner, D.J. (1998) Thermoelastic equation of state of monoclinic pyroxene: $CaMgSi_2O_6$ diopside. Review of High Pressure Science and Technology, 7, 25–27.

MANUSCRIPT RECEIVED DECEMBER 26, 2001
MANUSCRIPT ACCEPTED SEPTEMBER 17, 2002
MANUSCRIPT HANDLED BY ALISON R. PAWLEY